Published in final edited form as:
Biomaterials. 2013 March ; 34(9): 2194–2201. doi:10.1016/j.biomaterials.2012.11.061.

Effects of Cerium Oxide Nanoparticles on the Growth of Keratinocytes, Fibroblasts and Vascular Endothelial Cells in Cutaneous Wound Healing

Srinivasulu Chigurupati[1,2], **Mohamed R. Mughal**[1], **Eitan Okun**[1], **Soumen Das**[2], **Amit Kumar**[2], **Michael McCaffery**[3], **Sudipta Seal**[2,*], and **Mark P. Mattson**[1,*]

[1]Laboratory of Neurosciences, National Institute on Aging Intramural Research Program, Baltimore, Maryland 21224, USA. And Department of Molecular Biology and Microbiology, Burnett School of Biomedical Science, University of Central Florida, Orlando, FL

[2]Advanced Materials Processing and Analysis Centre, Nanoscience Technology Center (NSTC), Mechanical Materials Aerospace Eng, University of Central Florida, Orlando, Florida 32816, USA

[3]The Integrated Imaging Center, Department of Biology, Engineering in Oncology Center and The Institute of NanoBiotechnology, Johns Hopkins University, Baltimore MD 21218

Abstract

Rapid and effective wound healing requires a coordinated cellular response involving fibroblasts, keratinocytes and vascular endothelial cells (VECs). Impaired wound healing can result in multiple adverse health outcomes and, although antibiotics can forestall infection, treatments that accelerate wound healing are lacking. We now report that topical application of water soluble cerium oxide nanoparticles (Nanoceria) accelerates the healing of full-thickness dermal wounds in mice by a mechanism that involves enhancement of the proliferation and migration of fibroblasts, keratinocytes and VECs. The Nanoceria penetrated into the wound tissue and reduced oxidative damage to cellular membranes and proteins, suggesting a therapeutic potential for topical treatment of wounds with antioxidant nanoparticles.

Keywords

Cerium oxide nanoparticles; angiogenesis; vascular endothelial cells; keratinocytes; fibroblasts; wound healing; oxidative stress

1. Introduction

Impaired wound healing and its medical complications result in a large burden of morbidity and mortality worldwide. Wound repair requires the proliferation and migration of fibroblasts and keratinocytes which re-establish the normal cellular and extracellular matrix composition of skin, and the growth of vascular endothelial cells (VECs) to form new blood vessels that supply nutrients to the skin cells [1]. The ability of all three cell types to restore skin integrity and function is compromised in non-healing wounds, and one factor that

*Correspondence should be addressed to Mark P. Mattson: mattsonm@grc.nia.nih.gov or Sudipta Seal: Sudipta.Seal@ucf.edu.

contributes to such impaired wound healing is sustained oxidative stress [2]. Cells within and surrounding wounds experience elevated levels of superoxide, hydrogen peroxide and nitric oxide, and proteins modified by nitration and the lipid peroxidation product 4-hydroxynonenal. Levels of endogenous antioxidants such as glutathione and vitamin E are diminished under conditions that impair wound healing including aging and diabetes [3]. The potential for exogenous antioxidants to enhance wound healing has been tested in only a few studies using animal models with variable results [4–7].

The antioxidant capacity of cerium oxide nanoperticles (Nanoceria) has been explored recently; nanoceria were reported to scavenge superoxide radical [8, 9], hydrogen peroxide [10], hydroxyl radical [11] and nitric oxide radical [12]. Therefore, Nanoceria have been tested in biological systems to protect tissues against radiation induced damage [13], protect against laser-induced retinal damage [14], increase life span of photoreceptor cells [15], reduce spinal injury [16], reducte chronic inflammation [17] and promote angiogenesis [18]. In this study we explore the potential theraputic effect of Nanoceria in an animal model of wound healing.

2. Materials & Methods

2.1. Synthesis and characterization of Nanoceria

Cerium oxide nanoparticles were synthesized using wet chemistry methods as described previously [19]. Briefly, stoichiometric amounts of cerium nitrate hexahydrate (99.999% pure from Sigma Aldrich) was dissolved in deionized water. The solution was oxidized using excess hydrogen peroxide. After the synthesis of nanoparticles, the pH of the solution was maintained below 3.0 using 1 N nitric acid to keep the Nanoceria in suspension. The size and morphology of the nanoceria were evaluated using High resolution transmission electron microscopy (HRTEM), with FEI Tecnai F30 EDX analyzer. X-ray photon spectrometer 5400 PHI ESCA (XPS) with Mg-Kα X-radiation (1253.6 eV) at a power of 350watts was used to analyze the surface property and oxidation state of Nanoceria. X-ray diffraction (XRD) was carrying out using monochromatized CuKα radiation.

2.2. Cell cultures

Human keratinocyte cells were obtained from ATCC and grown in keratinocyte medium containing 0.05 mg/ml bovine pituitary extract and 5 ng/ml epidermal growth factor (Invitrogen). Skin tissue explants established from young adult mice were used to harvest fibroblasts. Dermal tissue specimens were cut into ~3–5 mm pieces. These fragments were placed on the surface of 100 mm Petri dishes for 40–50 minutes to allow adherence of the tissue to the culture surface. Ten ml of DMEM with 20% fetal bovine serum, 100 IU/ml penicillin and 100 mg/ml streptomycin (pH 7.6; 37°C), was gently added to the culture dishes. Cultures were maintained in a humidified incubator at 37°C in a 5% CO2/95% air atmosphere. Cultures were passaged on reaching 75–80% confluence, using 0.05% trypsin/EDTA (Invitrogen) and the medium was changed every two days. Cells were used at passage 4 or 5 for cell migration and proliferation assays in order to minimize the influence of genetic alterations and senescent changes. Human microvascular endothelial cells (HMEC-1 cells) were kindly provided by Fransisco Candal (Centers for Disease Control, Atlanta, GA). The latter cells are of human dermal microvascular origin and retain the morphologic, phenotypic, and functional features of normal human microvascular endothelial cells [20]. HMEC-1 cells were maintained in MCDB 131 formula (Invitrogen) supplemented with 10% fetal bovine serum, 10 ng/ml epidermal growth factor, 1 mg/ml hydrocortisone and 10 mM L-glutamine.

2.3. Full-thickness skin wounds and quantification of healing

These methods were similar to those described previously [7]. All experiments were performed using 3–4 month-old male C57BL/6 mice. Mice were anesthetized using 2% vaporized inhaled isoflurane and the dorsal skin was cleansed with Betadine. Two full-thickness wounds were created in the skin on the back of each mouse using a 4 mm diameter biopsy punch (Miltex Instrument, York, PA, USA) and a biotome (Acu Punch, Acuderm Inc., Fort Lauderdale, FL, USA). Mice were treated with vehicle (10 μl of deionized water) or 10 μl of a 10 μM solution of Nanoceria applied directly to the wound site once daily. Some mice in each group were euthanized on days 1, 3, 5, 8 and 13 post-wounding, and skin tissue samples from the wound site were collected from all of the mice for histological and biochemical analyses. Some mice from each treatment group (n= 6) were evaluated daily for 13 days following wounding. Digital photographs of the injury site were taken with a standard-sized dot placed beside the wound; wound size was expressed as the ratio of the wound area to the dot measurement. Measurements of wound length and width were obtained using a caliper. The first post-incision wound measurement was made on day 0. The measurements were done without knowledge of the treatment history of the mice. Wound area was calculated using digital planimetry; linear healing progress was determined using the standard formula [7].

2.4. Histological examination

Biopsy specimens that included the central part of the wounds (days 1, 3 5, 8 and 13) were obtained perpendicularly to the dorsal midline from mice for light microscopy. Skin specimens were fixed in formalin, dehydrated through a graded ethanol concentration series, cleared in xylene, and embedded in paraffin wax. Sections were cut at 5 μm thickness using a vibratome, and were stained with hematoxylin and eosin. The histomorphometric method was an adaptation of the point-counting procedure. The counting of mononuclear inflammatory cells and blood vessels was performed at a total magnification of 200 in 3 random fields per section limited to the wounded area. Images were acquired using a Nikon Eclipse 80i microscope and images were analyzed using IP lab software (BD Biosciences Bio-imaging, Rockville, MD). After acquiring transmitted light images, a 252-square graticule was superimposed on the screen over the wounded site to facilitate counting. A standard histologic grading system was used to evaluate cellular aspects of the wound healing process. All the slides were evaluated by a veterinary pathologist (S. C.) in a blinded manner.

2.5. Immunoblot analysis

Proteins were extracted from skin tissue samples using T-PER tissue protein extraction buffer with protease inhibitor cocktail (Sigma). Methods for protein quantification, electrophoretic separation of proteins, and transfer of the proteins to nitrocellulose membranes have been described previously [21]. Membranes were incubated in blocking solution (1% BSA in Tween Tris-buffered saline; TTBS) overnight at 4°C followed by a 1 h incubation in primary antibody diluted in blocking solution at room temperature. Membranes were then incubated for 1 hour in secondary antibody conjugated to horseradish peroxidase and bands were visualized using a chemiluminiscence detection kit (ECL, Amersham). The primary antibodies were a mouse monoclonal selective for proteins that are covalently modified by HNE on lysine residues [22] and a β-tubulin antibody (Sigma).

2.6. Immunofluorescence

Tissue samples were embedded in Optimal Cutting Temperature (OCT) compound and frozen. Sections (6 μm diameter) were cut with a cryostat and fixed in acetone. Subsequently sections were blocked with 10% goat serum before being incubated with rabbit anti- α

smooth muscle actin (1:200; Abcam) and mouse anti-nitrotyrosine (1:200; Zymed) overnight at 4°C. After being washed, the sections were incubated in anti-rabbit or anti mouse IgG conjugated to Alexa 568 and 488 (1:200 dilution), respectively for 45 min at room temperature. Sections were counterstained with Hoechst 33342 (Invitrogen) visualized under a Nikon Eclipse 80i microscope. Using calibrated images the total area of positive pixel intensity was measured and analyzed with two-way ANOVA (Newman-Keuls post hoc tests for pair wise comparisons) using GraphPad Prism version 5.00 for Windows, GraphPad Software, San Diego CA, USA.

2.7. Endothelial cell scratch wound healing assay

HMEC-1 cells, human keratinocytes and mouse fibroblasts were seeded into 60 mm plates and grown to confluency. After 24 hours of serum starvation (DMEM supplemented with 1% FBS), cells were treated with either vehicle or Nanoceria (500 nM, 1 and 10 μM). The cell monolayer was then damaged by scratching with a sterile 200 μl pipette tip. Cells were then cultured for additional period of 24 hours in a serum-free basal medium in the continued presence of vehicle or Nanoceria. Cells were then fixed in a solution of 4% paraformaldehyde in PBS and stained with crystal violet. Cells in the injury area were visualized under phase-contrast optics (10X objective) and the number of cells which had migrated into the initially cell-free scratch area was counted.

2.8. Endothelial tube formation and chemotaxis cell migration assays

HMEC-1 cells (1×10^3 cells/well) were dispensed to Matrigel-coated 8-well chamber slides (Lab-Tek, Nalge Nunc International, Rochester, NY, USA) in 125 ml of EGM-2 medium containing either vehicle or Nanoceria (500 nM, 1 and 10 μM) and incubated for 18 hours. The cells were then visualized by microscopy and tube formation was quantified as described previously [7]. Analysis of migration of keratinocytes, fibroblasts and HMEC-1 cells was performed using Transwell membrane filters (Corning, Costar) containing a polycarbonate filter with 8 mm pores. The bottom chamber was filled with complete growth medium containing chemoattractant growth factors. Cells (5×10^4 in 100 μl) were seeded into each transwell with EGM containing 0.2% fetal bovine serum with vehicle or Nanoceria (500 nM, 1 and 10 μM) and allowed to migrate for 6 hours. At the end of the incubation, non-migrated cells remaining in the transwell insert were removed. The migrated cells (on the outer bottom of the transwell) were fixed with methanol and stained with hematoxylin and eosin. The stained cells were counted in 5 or more random 100X fields. Each experiment was performed in triplicate, and the experiment was repeated twice. Growth correction was not applied because a significant increase in the cell number did not occur during the incubation period of 6 hours.

2.9. Cell proliferation assay

The proliferation of cultured endothelial cells, keratinocytes and fibroblasts was measured using a colorimetric assay. Cells (1×10^4) were incubated with either vehicle or Nanoceria (500 nM, 1 and 10 μM) for 24, 48 or 72 hours. Ten microliters of 3-(4, 5-dimethylthiazol-2-yl)-2,5-diphenyl-2H-tetrazolium bromide solution (R&D Systems Inc. Minneapolis, MN) was added to each well and the cells were incubated for a further 4 hours at 37°C. After the cells were washed 3 times with PBS (pH 7.4), the insoluble formazan product was dissolved by incubation with 100 μl detergent for 2 hours. The absorbance of each well was measured on an enzyme-linked immunosorbent assay (ELISA) micro-plate reader at 570 nm. Each experiment was performed in quadruplicate. The cell proliferation rate was calculated as absorbance Nanoceria-treated cultures/absorbance control cultures × 100.

2.10. Statistical analyses

All values are expressed as the mean and SEM. Data were analyzed by ANOVA with Newman-Keuls post-hoc tests for pair-wise comparisons using GraphPad Prism version 5.00 for Windows (GraphPad Software, San Diego California USA).

3. Results

Shape, size and physiochemical properties of nanoparticles are very important for biological applications, and we therefore engineered nanoparticles within a size range of 3—5 nm (Figure 1A), with agglomeration size ≤50 nm (data not shown). The selected area electron diffraction pattern (SADE) of nanoceria confirmed their crystalline nature and fluorite structure (Figure 1B); 111, 200, 220, 311, 222 and 400 in the SAED correspond to the different lattice planes of Nanoceria fluorite crystal structure. The X-ray diffraction pattern of the Nanoceria showed the particles are crystalline with typical peak broadening characteristic of nano size particles (Figure 1C). These optimally engineered Nanoceria were used in this study.

Cultured primary skin keratinocytes and fibroblasts were treated with vehicle or increasing concentrations of Nanoceria (500 nM, 1 μM and 10 μM), and migration and proliferation of the cells were quantified using established methods [7]. The migration of both the keratinocytes and fibroblasts was increased significantly in cells treated with 1 and 10 μM Nanoceria, but not in cells treated with no or 500 nM Nanoceria (Figure 2A, B). We next quantified cell growth/proliferation during a 3 day period in control and Nanoceria-treated keratinocytes and fibroblasts. The growth rate of both cell types was significantly increased in cells treated with 1 and 10 μM Nanoceria compared to cultures treated with 500 nM or no Nanoceria (Figure 2 C, D).

In addition to the growth of epidermal keratinocytes and dermal fibroblasts into the wound site, proper wound healing requires neovascularization of the newly-generated dermis, a process involving the proliferation and migration of VEC [23]. VEC treated with 1 and 10 μM Nanoceria exhibited up to a two-fold increase in their migration rate using a transwell chemoattraction assay (Figure 2E), and a highly significant increase in their migration rate using a scrape assay (Figure 2F). In addition, the growth rate of the VEC was significantly increased during a 3 day period of exposure to 1 and 10 μM Nanoceria compared to VEC treated with vehicle or 500 nM Nanoceria (Figure 2G). In order to form blood vessels, the VEC must form tubes. When grown in a three dimensional Matrigel matrix, the formation of tubes by the VEC was significantly increased by more than 3-fold in cells treated with 1 and 10 μM Nanoceria (Figure 2H, I).

We next determined whether topical application of Nanoceria would accelerate wound healing processes using a model of skin wound healing in mice [7]. Two full-thickness dermal wounds were made in the skin on the back of adult C57BL/6 mice using a skin biopsy punch. Nanoceria (10 μl of a 10 μM solution) or vehicle were applied to the wounds once daily, and wound size was quantified from images taken on post-wounding days 1, 3, 5, 8 and 13. In control mice the wound size decreased progressively with an average diameter of 3.6 mm on day 1 and an average diameter of 1.2 mm on day 13 (Figure 3). The rate of wound closure in mice treated with Nanoceria was significantly faster than the rate of control mice, with the wounds in all Nanoceria-treated mice being completely closed on days 8 and 13 (Figure 3).

To elucidate the cellular changes underlying the accelerated healing of wounds treated with Nanoceria, we immunostained tissue sections of the wound area with an antibody to α-smooth muscle actin, a marker of differentiated myofibroblasts. Levels of α-smooth muscle

actin immunoreactivity were significantly greater in Nanoceria-treated mice compared to vehicletreated control mice on post-wound days 5, 8 and 13 (Figure 4 A, B) suggesting that Nanoceria enhance myofibroblast differentiation.

The rapid infiltration of leukocytes into the wound area plays an important role in preventing infection and clearing debris, thereby enabling migration of keratinocytes and fibroblasts, and vascularization of the new skin tissue [24]. We therefore counted mononuclear leukocytes in the wound tissue of control and Nanoceria-treated at post-injury day 5. There were approximately 3-fold more leukocytes in the wounds of Nanoceria-treated mice compared to control mice (Figure 4 C). To evaluate neovascularization of the wounds we quantified the number of blood vessels in skin tissue sections stained with hematoxylin and eosin. The density of blood vessels was significantly greater in the healing wounds of Nanoceria-treated mice compared to control mice (Figure 4 D).

Because Nanoceria are known to scavenge reactive oxygen species, and because excessive oxidative stress can impair wound healing, we measured levels of two different markers of oxidative stress in wound tissue samples from mice that had been treated with either vehicle or Nanoceria (10 μM). First, we performed immunoblot analysis of protein in samples from wound tissue taken at 1, 3, 5, 8 and 13 days post-injury, using an antibody against proteins covalently modified by the lipid peroxidation product 4-hydroxynonenal (HNE). Levels of HNE-protein adducts were significantly lower in wound tissue samples from Nanoceria-treated mice compared to control mice at all post-wound time points (Figure 5 A). Peroxynitrite, which is formed by the interaction of superoxide with nitric oxide, can cause nitration of proteins on tyrosine residues, an oxidative modification that can be detected using specific antinitrotyrosine antibodies [25]. We found that levels of nitrotryosine were significantly lower in wound tissues samples from Nanoceria-treated mice compared to control mice at all post-injury time points (Figure 5 B). Transmission electron microscopy was used to confirm that the Nanoceria did, in fact, accumulate within and surrounding the cells within the wound site (Figure 5 C).

4. Discussion

Cerium oxide nanoparticles (Nanoceria) can scavenge superoxide with a catalytic rate greater than cellular superoxide dismutase [9]. It was recently reported that Nanoceria enter cultured keratinocytes via clathrin-mediated endocytosis and are then distributed to multiple subcellular compartments including the cytoplasm, mitochondria, endoplasmic reticulum and nucleus [26]. We therefore determined whether Nanoceria exert biological actions on cells involved in wound healing.

Our cell culture studies demonstrated that engineered Nanoceria with 3–5 nm size at low micromolar concentrations enhance the proliferation and migration of keratinocytes and fibroblasts, and accelerate the migration and tube-forming ability of vascular endothelial cells. Daily topical application of Nanoceria to full-thickness dermal wounds accelerated healing without altering the normal cellular remodeling involved in the healing process. Previous studies demonstrated that Nanoceria possess superoxide dismutase activity [27] and can inhibit the production of nitric oxide and inflammatory cytokines in cultured macrophages [17]. Consistent with an antioxidant mechanism of action, we found that Nanoceria attenuated the accumulation of HNE- and nitrotyrosine-modified proteins in the wound tissue.

A previous study suggested a mechanism by which Nanoceria can enhance angiogenesis; Nanoceria modulate the intracellular oxygen environment so as to stabilize hypoxia inducing factor 1α and increase the production of VEGF [28]. Concomitant with the latter effects of

Nanoceria is enhancement of endothelial cell proliferation and tube formation in cell culture and in-vivo vascular sprouting. Additional data in the latter study suggest that the surface reactivity of CNPs and facile oxygen transport promotes angiogenesis. In the present study we found that Nanoceria treatment results in a reduction in markers of oxidative stress in cultured vascular endothelial cells. The available data therefore indicate Nanoceria promote angiogenesis by a mechanism independent of production of reactive oxygen species including nitric oxide.

Dynamic mechanisms involving multiple cell types are involved in wound healing, and it is unlikely that Nanoceria control all aspects of the wound healing process. Our findings suggest that engineered Nanoceria facilitate the proliferation of cultured microvascular endothelial cells, keratinocytes and fibroblasts, and their migration. These three cell types undoubtedly receive numerous signals from different cells and extracellular matrix cues during the wound healing process. Presumably the Nanoceria do not prevent the responses of fibroblasts, keratinocytes and endothelial cells to such signals and therefore permit a normal sequence of dynamic events with regards to cell proliferation, migration and stabilization of the newly generated skin. We have added this consideration to the Discussion of the revised manuscript.

We found that Nanoceria enhanced leukocyte infiltration into the wound tissue during the first 5 days after the injury. Together with the accelerated and complete healing of the skin wound, the latter finding suggests that Nanoceria treatment does not compromise the immune killing of pathogens and the clearance of debris from the wound. Prooxidants can reduce infection, but may inhibit healing of wounds, and reduced levels of endogenous antioxidants are associated with impaired wound healing [2, 29]. Only a few antioxidants have been reported effective in enhancing wound healing in animal models, and thus far only one antioxidant (Medihoney) has been approved by the Food and Drug Administration [30].

Nanoceria can reduce damage to retinal photoreceptors and associated visual impairment resulting from exposure to intense light by a mechanism involving reduced cellular oxidative stress [14]. Recent findings suggest that Nanoceria can be administered intravascularly to mice with no discernable side effects, and with a therapeutic benefit to photoreceptor cells in a mouse model of genetically determined retinal degeneration [31]. Silver nanoparticles exhibit antibacterial activity and can improve the healing of wounds [32]. In addition, recent findings suggest that carbon fullerene nanoparticles can enhance wound healing [33]. The ability of topical application of Nanoceria to accelerate wound healing in an animal model provides a rationale to develop this technology for use in humans affected by traumatic injury, diabetes and burns.

5. Conclusion

In summary, we have shown that a simple topical application of water soluble Nanoceria accelerates the healing of full-thickness dermal wounds in a mice model. In particular engineered Nanoceria formulation enhances the proliferation and migration of fibroblasts, keratinocytes and VECs cells which further accelerate the wound healing process. Moreover, Nanoceria reduce the oxidative stress in wounded region and protect regenerative tissue. This study suggests the therapeutic potential for topical treatment of wounds with regenerative engineered antioxidant Nanoceria particles.

Acknowledgments

This research was supported by the National Institute on Aging Intramural Research Program of the NIH. SS acknowledges the grant from National Science Foundation (NIRT: CBET) for funding the nanotechnology research.

References

1. Barrientos S, Stojadinovic O, Golinko MS, Brem H, Tomic-Canic M. Growth factors and cytokines in wound healing. Wound Repair Regen. 2008; 16:585–601. [PubMed: 19128254]
2. Schafer M, Werner S. Oxidative stress in normal and impaired wound repair. Pharmacol Res. 2008; 58:165–171. [PubMed: 18617006]
3. Rasik AM, Shukla A. Antioxidant status in delayed healing type of wounds. Int J Exp Pathol. 2000; 81:257–263. [PubMed: 10971747]
4. Pehr K, Forsey RR. Why don't we use vitamin E in dermatology? CMAJ. 1993; 149:1247–1253. [PubMed: 8221479]
5. Sidhu GS, Singh AK, Thaloor D, Banaudha KK, Patnaik GK, Srimal RC, et al. Enhancement of wound healing by curcumin in animals. Wound Repair Regen. 1998; 6:167–177. [PubMed: 9776860]
6. Lateef H, Aslam MN, Stevens MJ, Varani J. Pretreatment of diabetic rats with lipoic acid improves healing of subsequently-induced abrasion wounds. Arch Dermatol Res. 2005; 297:75–83. [PubMed: 15986218]
7. Chigurupati S, Mughal MR, Chan SL, Arumugam TV, Baharani A, Tang SC, et al. A synthetic uric acid analog accelerates cutaneous wound healing in mice. PLoS One. 2010; 5:e10044. [PubMed: 20386608]
8. Karakoti A, Singh S, Dowding JM, Seal S, Self WT. Redox-active radical scavenging nanomaterials. Chem Soc Rev. 2010; 39:4422–4432. [PubMed: 20717560]
9. Korsvik C, Patil S, Seal S, Self WT. Superoxide dismutase mimetic properties exhibited by vacancy engineered ceria nanoparticles. Chem Commum. 2007:1056–1058.
10. Pirmohamed T, Dowding JM, Singh S, Wasserman B, Heckert E, Karakoti AS, et al. Nanoceria exhibit redox state-dependent catalase mimetic activity. Chem Commun. 2010; 46:2736–2738.
11. Xue Y, Luan Q, Yang D, Yao X, Zhou K. Direct Evidence for Hydroxyl Radical Scavenging Activity of Cerium Oxide Nanoparticles. J Phys Chem C. 2011; 115:4433–4438.
12. Dowding JM, Dosani T, Kumar A, Seal S, Self WT. Cerium oxide nanoparticles scavenge nitric oxide radical ([radical dot]NO). Chem Commun. 2012; 48:4896–4898.
13. Tarnuzzer RW, Colon J, Patil S, Seal S. Vacancy engineered ceria nanostructures for protection from radiation-induced cellular damage. Nano Letters. 2005; 5:2573–2577. [PubMed: 16351218]
14. Chen J, Patil S, Seal S, McGinnis JF. Rare earth nanoparticles prevent retinal degeneration induced by intracellular peroxides. Nat Nanotechnol. 2006; 1:142–150. [PubMed: 18654167]
15. Cai X, Sezate SA, Seal S, McGinnis JF. Sustained protection against photoreceptor degeneration in tubby mice by intravitreal injection of nanoceria. Biomaterials.
16. Das M, Patil S, Bhargava N, Kang JF, Riedel LM, Seal S, et al. Auto-catalytic ceria nanoparticles offer neuroprotection to adult rat spinal cord neurons. Biomaterials. 2007; 28:1918–1925. [PubMed: 17222903]
17. Hirst SM, Karakoti AS, Tyler RD, Sriranganathan N, Seal S, Reilly CM. Anti-inflammatory properties of cerium oxide nanoparticles. Small. 2009; 5:2848–2856. [PubMed: 19802857]
18. Das S, Singh S, Dowding JM, Oommen S, Kumar A, Sayle TXT, et al. The induction of angiogenesis by cerium oxide nanoparticles through the modulation of oxygen in intracellular environments. Biomaterials. 2012; 33:7746–7755. [PubMed: 22858004]
19. Karakoti AS, Monteiro-Riviere NA, Aggarwal R, Davis JP, Narayan RJ, Self WT, et al. Nanoceria as Antioxidant: Synthesis and Biomedical Applications. JOM (1989). 2008; 60:33–37. [PubMed: 20617106]

20. Ades EW, Candal FJ, Swerlick RA, George VG, Summers S, Bosse DC, Lawley TJ. HMEC-1: establishment of an immortalized human microvascular endothelial cell line. J Invest Dermatol. 1992; 99:683–690. [PubMed: 1361507]
21. Kyriazis GA, Wei Z, Vandermey M, Jo DG, Xin O, Mattson MP, et al. Numb endocytic adapter proteins regulate the transport and processing of the amyloid precursor protein in an isoform-dependent manner: implications for Alzheimer disease pathogenesis. J Biol Chem. 2008; 283:25492–25502. [PubMed: 18599481]
22. Waeg G, Dimsity G, Esterbauer H. Monoclonal antibodies for detection of 4-hydroxynonenal modified proteins. Free Radic Res. 1996; 25:149–159. [PubMed: 8885333]
23. Eming SA, Brachvogel B, Odorisio T, Koch M. Regulation of angiogenesis: wound healing as a model. Prog Histochem Cytochem. 2007; 42:115–170. [PubMed: 17980716]
24. Martin P, Leibovich SJ. Inflammatory cells during wound repair: the good, the bad and the ugly. Trends Cell Biol. 2005; 15:599–607. [PubMed: 16202600]
25. Fadini GP, Albiero M, Menegazzo L, Boscaro E, Pagnin E, Iori E, et al. The redox enzyme p66Shc contributes to diabetes and ischemia-induced delay in cutaneous wound healing. Diabetes. 2010; 59:2306–2314. [PubMed: 20566667]
26. Singh S, Kumar A, Karakoti A, Seal S, Self WT. Unveiling the mechanism of uptake and sub-cellular distribution of cerium oxide nanoparticles. Mol Biosyst. 2010; 6:1813–1820. [PubMed: 20697616]
27. Heckert EG, Karakoti AS, Seal S, Self WT. The role of cerium redox state in the SOD mimetic activity of nanoceria. Biomaterials. 2008; 29:2705–2709. [PubMed: 18395249]
28. Das S, Singh S, Dowding JM, Oommen S, Kumar A, Sayle TX, Saraf S, Patra CR, Vlahakis NE, Sayle DC, Self WT, Seal S. The induction of angiogenesis by cerium oxide nanoparticles through the modulation of oxygen in intracellular environments. Biomaterials. 2012; 33:7746–7755. [PubMed: 22858004]
29. Menke NB, Ward KR, Witten TM, Bonchev DG, Diegelmann RF. Impaired wound healing. Clin Dermatol. 2007; 25:19–25. [PubMed: 17276197]
30. Fitzmaurice SD, Sivamani RK, Isseroff RR. Antioxidant therapies for wound healing: a clinical guide to currently commercially available products. Skin Pharmacol Physiol. 2011; 24:113–126. [PubMed: 21242718]
31. Kong L, Cai X, Zhou X, Wong LL, Karakoti AS, Seal S, et al. Nanoceria extend photoreceptor cell lifespan in tubby mice by modulation of apoptosis/survival signaling pathways. Neurobiol Dis. 2011; 42:514–523. [PubMed: 21396448]
32. Chaloupka K, Malam Y, Seifalian AM. Nanosilver as a new generation of nanoproduct in biomedical applications. Trends Biotechnol. 2010; 28:580–588. [PubMed: 20724010]
33. Zhou Z, Joslin S, Dellinger A, Ehrich M, Brooks B, Ren Q, et al. A novel class of compounds with cutaneous wound healing properties. J Biomed Nanotechnol. 2010; 6:605–611. [PubMed: 21329053]

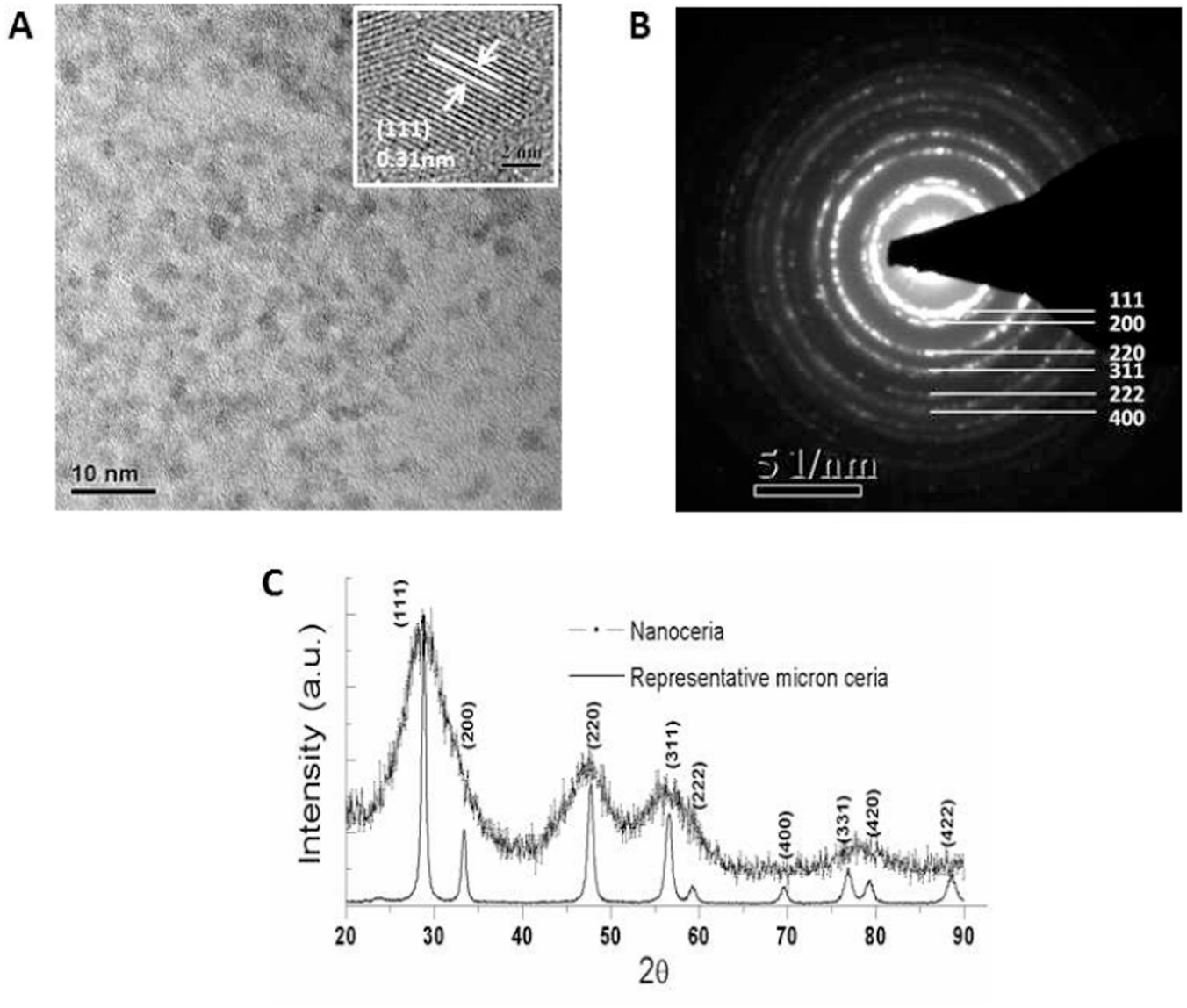

Figure 1.

Characterization of Nanoceria. **A.** HRTEM image showing the homogeneous distribution of size and shape of Nanoceria, inset higher magnification image of nanoceria reveling the size range in between 3–5nm. **B.** The selected area electron diffraction pattern (SADE) of Nanoceria confirms the crystalline nature and fluorite structure; 111, 200, 220, 311, 222 and 400 correspond to the different lattice planes of nanoceria. **C.** XRD data of Nanoceria, further confirm the crystalline nature of the nanoparticle.

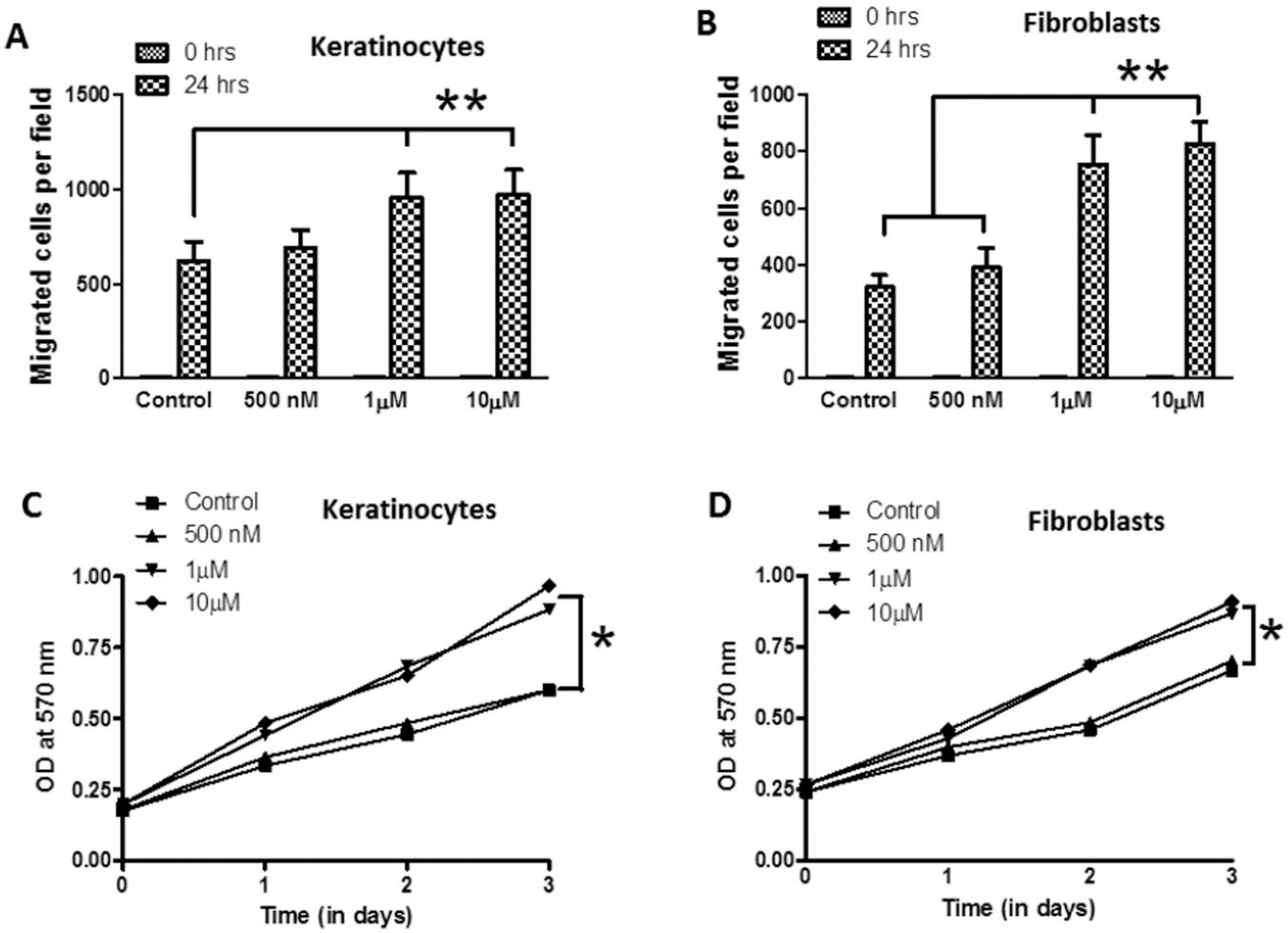

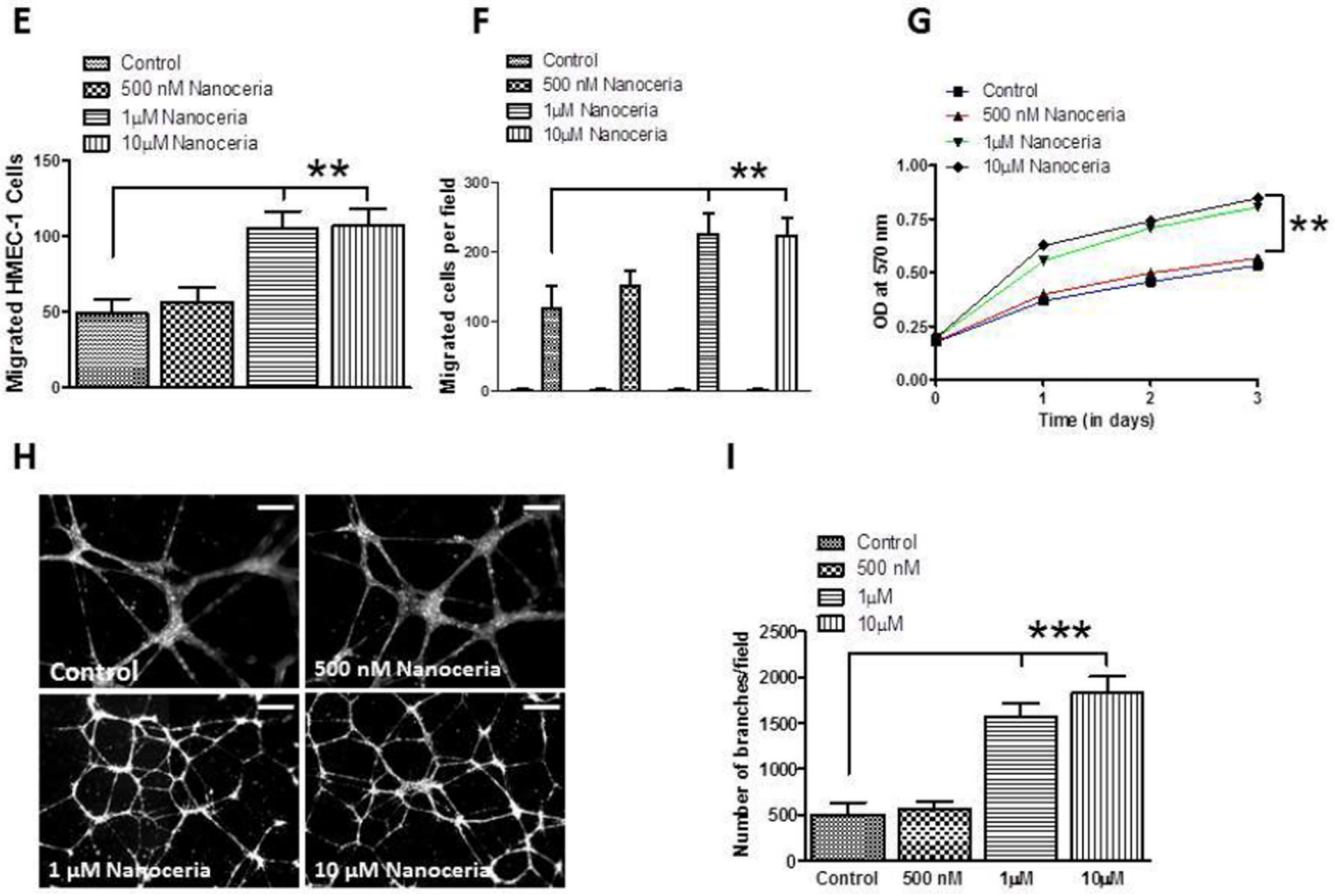

Figure 2.

Nanoceria enhance the motility and/or proliferation of keratinocytes, fibroblasts and vascular endothelial cells. **A and B.** Monolayers of cultured keratinocytes (A) and fibroblasts (B) were treated with vehicle (Control) or Nanoceria (500 nM, 1 and 10 μM), and were then subjected to scratch wounding. Eighteen hours after wounding, images of the wound area were acquired and the number of cells per field that had migrated into the cell-free wound zone was determined for each culture. *$p<0.01$ (n = 4 separate experiments). **C and D.** Cultured keratinocytes (C) and fibroblasts (D) were treated with vehicle (Control) or Nanoceria (500 nM, 1 and 10 μM) for the indicated time periods and relative cell numbers were estimated by O.D readings. *$p<0.05$ (n = 6 experiments). **E**. Cultured HMEC-1 were treated with deionized water (control) or Nanoceria (500 nM, 1 and 10 μM) in conditioned medium and plated into chemo-attractant medium consisting of regular growth medium supplemented with 10% fetal bovine serum and growth factors, and cell migration was evaluated using a 24 well Transwell chamber assay. **$p<0.01$ (n = 4 experiments). **F.** HMEC-1 cell monolayers were mechanically wounded with the tip of 20–200 μl pipette tip following treatment without (control) or with Nanoceria (500 nM, 1 and 10 μM). **$p<0.01$ (n = 3 experiments). **G.** Cultured HMEC-1 cells were treated with vehicle or Nanoceria (500 nM, 1 and 10 μM) for the indicated time periods and relative cell numbers were quantified by O.D readings. *$p<0.001$ (n = 6 experiments). **H and I.** HMEC-1 cells were seeded on low growth factor-containing Matrigel-coated 8-well chamber slides and cultured in the presence of low-serum medium with vehicle (control) or Nanoceria (500 nM, 1 and 10 μM). Tube formation, designated as the number of branch points/100X field) was evaluated 18 h

after cell seeding. Representative images are shown in D and quantitative data in E. *p<0.001 (n = 10–12 cultures). Scale bars = 100 μm.

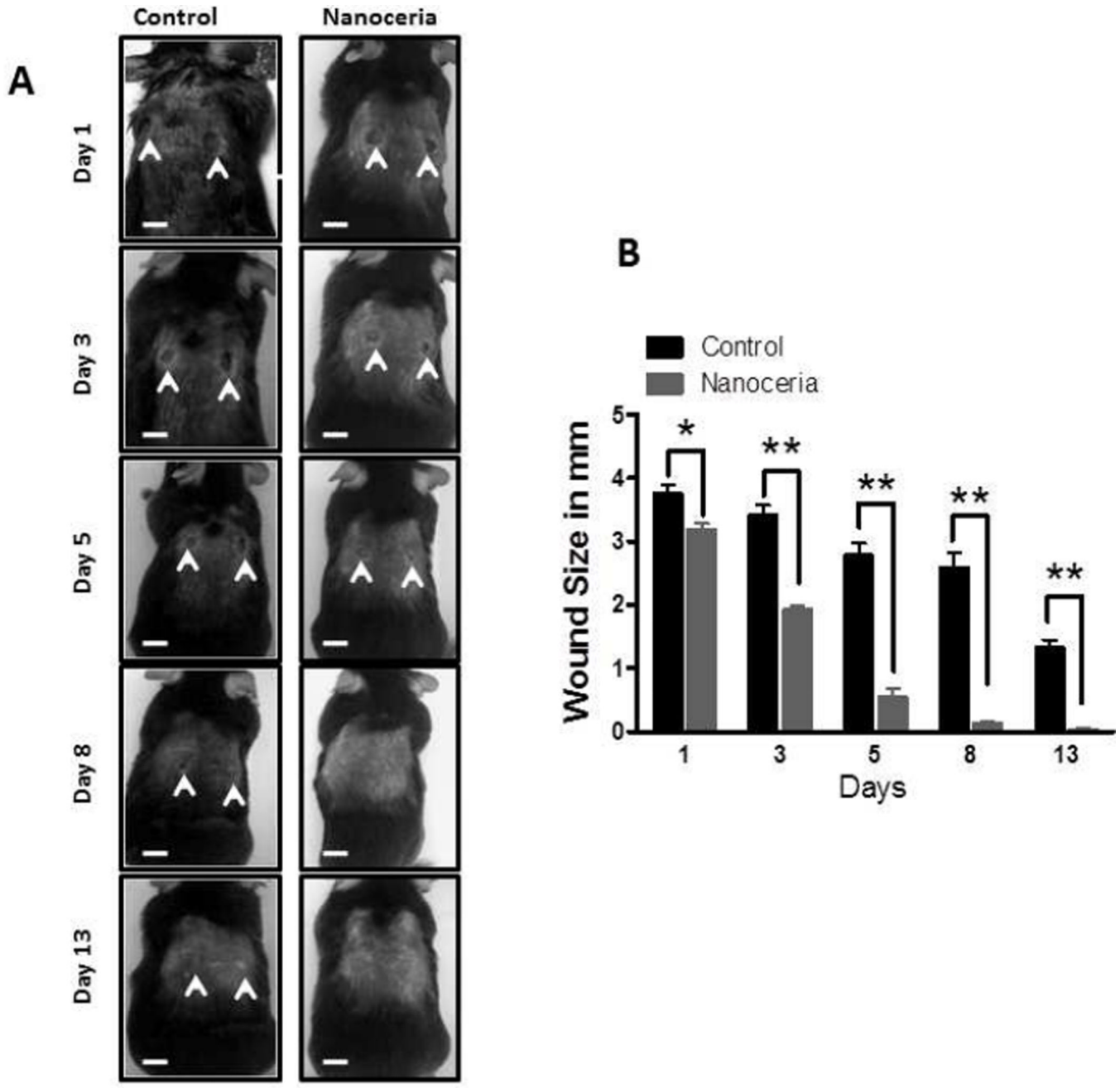

Figure 3.

Topical application of Nanoceria accelerates the healing of skin wounds in mice. Two full-thickness wounds were induced and then 10 μl of either vehicle (water) or 10 μM Nanoceria was applied to the wounds once daily for 13 days. **A.** Images of a representative mouse from each group taken on post-injury days 1, 3, 5, 8 and 13 are shown. **B.** Wound sizes at the indicated time points in control and Nanoceria-treated mice. **p<0.01, *p<0.05 (n = 6 mice per group). Scale bar = 4 mm.

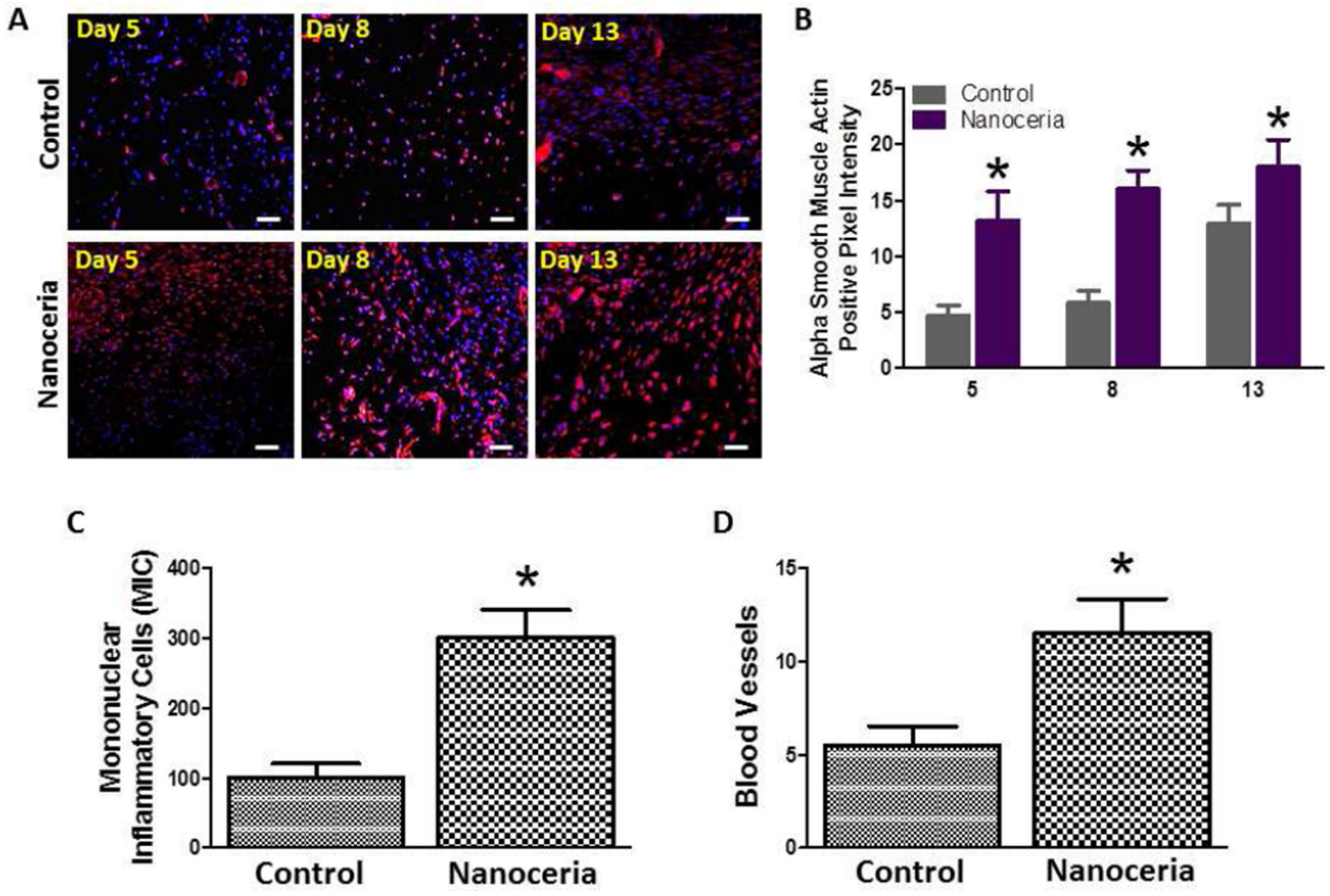

Figure 4.

A. Examples of images of wound tissue sections from control and Nanoceria-treated mice immunostained using an α smooth muscle actin antibody to label differentiating myofibroblasts. Scale bar = 25 μm. **B.** Results of quantitative analysis of a smooth muscle actin immunoreactivity in wound tissue sections from control and Nanoceria-treated mice at the indicated post-injury time points. *$p<0.05$ (n = 6 mice per group). **C and D**. Wounds treated with Nanoceria exhibit enhanced infiltration of immune cells and enhanced growth of blood vessels. Numbers of mononuclear immune cells (D) and blood vessels (E) in wound tissue 5 days after the injury in control and Nanoceria-treated mice. *$p<0.05$ (n = 6 mice per group).

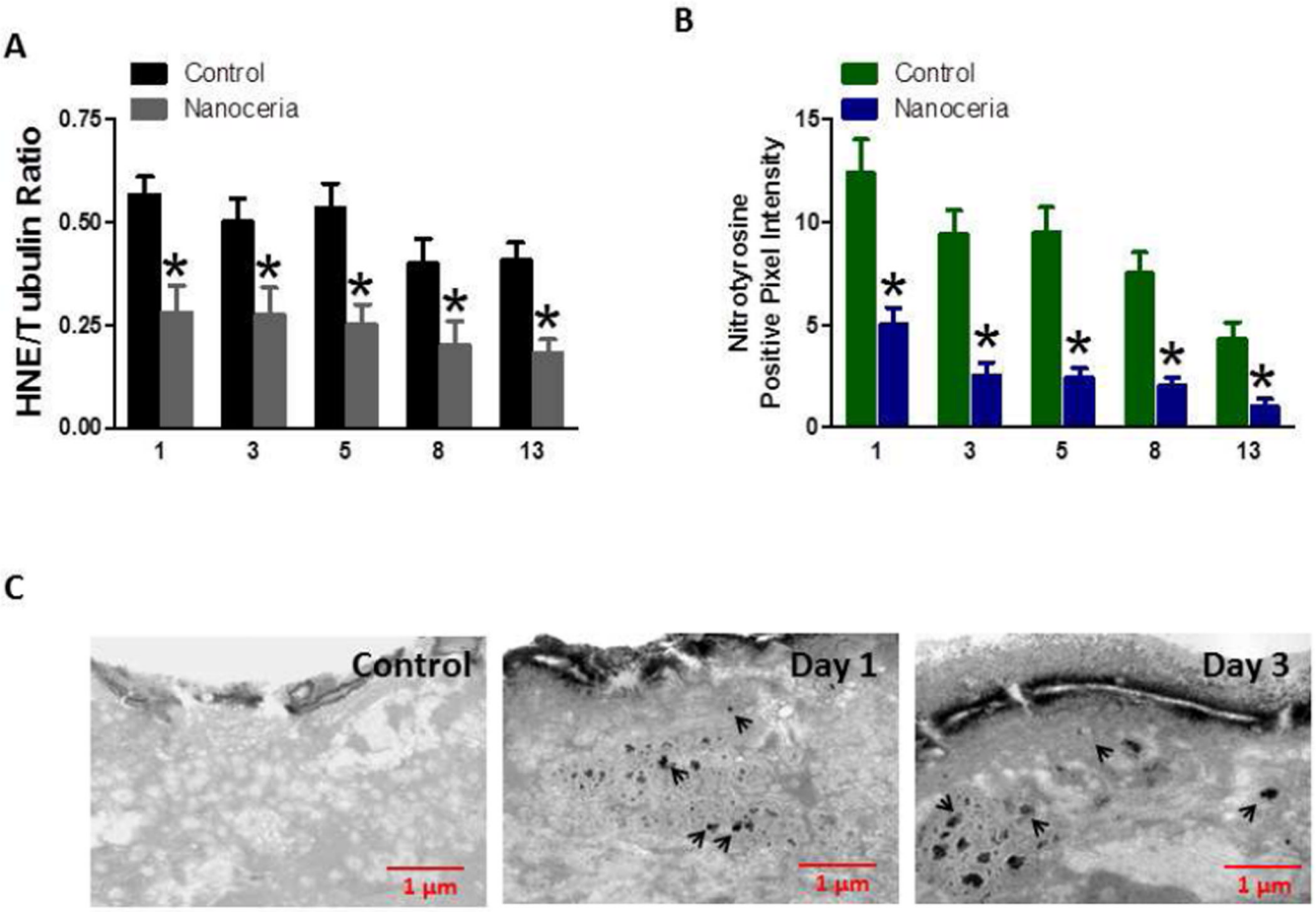

Figure 5.

Levels of proteins oxidatively modified by the lipid peroxidation product HNE and peroxynitrite in skin wounds are reduced in Nanoceria-treated mice compared to control mice. **A.** Levels of HNE-modified proteins in skin tissue samples from control and Nanoceria-treated mice at 1, 3, 5, 8, 13 days after injury. *$p<0.01$ (n = 4 mice per group). **B.** Levels of nitrated proteins (measured using an anti-nitrotyrosine antibody) in skin tissue samples from control and Nanoceria-treated mice atat 1, 3, 5, 8, 13 days after injury. *$p<0.001$ (n = 4 mice per group). **C.** Nanoceria accumulate outside of and within skin cells in dermal wounds. Transmission electron micrographs of skin biopsy samples from an unwounded control mouse (A), and mice that had been wounded either 1 or 3 days previously (B and C, respectively). Skin samples were taken 24 hours after application of Nanoceria.